IOPscience iopscience.iop.org

Home Search Collections Journals About Contact us My IOPscience

The magnetic phase diagram and transport properties of $FeGe_2$

This article has been downloaded from IOPscience. Please scroll down to see the full text article.

1997 J. Phys.: Condens. Matter 9 1347

(http://iopscience.iop.org/0953-8984/9/6/018)

View the table of contents for this issue, or go to the journal homepage for more

Download details:
IP Address: 171.66.16.207
The article was downloaded on 14/05/2010 at 08:04

Please note that terms and conditions apply.

J. Phys.: Condens. Matter **9** (1997) 1347–1355. Printed in the UK PII: S0953-8984(97)77735-X

The magnetic phase diagram and transport properties of $FeGe_2$

C P Adams, T E Mason, S A M Mentink and E Fawcett
Department of Physics, University of Toronto, Toronto, Ontario, Canada M5S 1A7

Received 10 September 1996

Abstract. We have used resistivity measurements to study the magnetic phase diagram of the itinerant antiferromagnet $FeGe_2$ in the temperature range from 0.3–300 K in magnetic fields up to 16 T. In contrast to theoretical predictions, the incommensurate spin-density-wave phase is found to be stable at least up to 16 T, with an estimated critical field $\mu_0 H_c$ of $\sim$30 T. We have also studied the low-temperature magnetoresistance in the [100], [110], and [001] directions. The transverse magnetoresistance is well described by a power law for magnetic fields above 1 T with no saturation observed at high fields. We discuss our results in terms of the magnetic structure and the calculated electronic band-structure of $FeGe_2$. We have also observed, for the first time in this compound, Shubnikov–de Haas oscillations in the transverse magnetoresistance with a frequency of 190 ± 10 T for a magnetic field along [001].

1. Introduction

There is growing evidence that the proximity of the high-T_c oxides to a spin-density-wave (SDW) instability is responsible for their anomalous normal-state transport properties [1] and possibly for the superconductivity itself [2–5]. This has led to a renewed interest in systems which exhibit similar instabilities since there are many unanswered questions regarding the transport and magnetic properties of SDW systems. The prototypical SDW systems are the itinerant antiferromagnet Cr and dilute alloys of Cr with other transition metals [6]. The tetragonal intermetallic compound $FeGe_2$ belongs to this class of materials and, in its undoped form, exhibits both commensurate and incommensurate magnetic ordering as temperature is varied. SDW ordering also occurs in Mott–Hubbard systems, such as $V_{2-y}O_3$, where strong correlations lead to a breakdown of conventional band theory and, as in the high-T_c cuprates, a metal–insulator transition [7].

The properties of $FeGe_2$ have been studied since 1943 and many of the details of the crystal and magnetic structure have been determined [8–11]. $FeGe_2$ is characterized by two magnetic phase transitions, the first of which is the Néel transition from a paramagnetic phase to an incommensurate SDW state at $T_N = 289$ K in zero field. The second one is a commensurate–incommensurate (C–IC) transition into a collinear antiferromagnetic structure. This transition occurs at $T_c = 263$ K in zero field. The propagation vector $\boldsymbol{Q}$ of the SDW is parallel to [100] and varies from 1 to roughly 1.05 a^* between the two transitions which are seen in resistivity [12, 13], ultrasonic attenuation [14], heat capacity [9, 15], and AC susceptibility [16] studies. A direct determination of the change in magnetic structure has been performed by elastic neutron scattering [9–11]. Theoretical predictions have been put forward as to the nature of the magnetic phase diagram [17, 18] and the magnetic parameters associated with it [19]. Although this compound has been well characterized in

0953-8984/97/061347+09$19.50 © 1997 IOP Publishing Ltd

zero field there has been very little work done in magnetic fields and not much is known about the details of the magnetic phase diagram.

This work explores the magnetic phase diagram and provides an experimental test of the theoretical predictions. We have used resistivity measurements along the [110] crystal direction in single-crystal $FeGe_2$ to find the phase transitions and determine the field and temperature dependences for fields up to 16 T along [110] and [100]. We find that the C–IC phase boundary rises steeply with magnetic field and would not intersect the Néel transition boundary until $\mu_0 H_c \simeq 30$ T for a simple extrapolation. This is in sharp contrast to theoretical predictions of $\mu_0 H_c \sim 1$ T [16]. We have also performed a detailed study of the low-temperature magnetoresistance of $FeGe_2$. The results reveal a moderate anisotropy between the *c*-axis and the basal plane and large differences in the longitudinal and transverse magnetoresistance. We have also observed Shubnikov–de Haas oscillations for a magnetic field along [001] at a frequency of 190 ± 10 T which had not been seen in previous de Haas–van Alpen experiments [20].

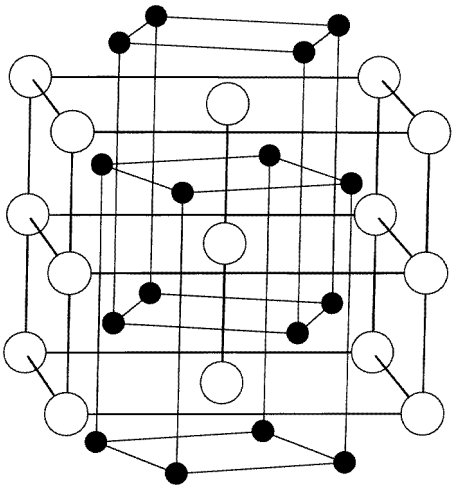

Figure 1. The crystal structure of $FeGe_2$. We show the unit cell defined by the Fe atoms (○) with the *c*-axis in the vertical direction. We can see that the Ge atoms (●) lie in the basal plane with a glide transformation connecting the neighbouring layers.

$FeGe_2$ has a tetragonal $CuAl_2$ structure with symmetry group D_{4h}^{18}, and space group $I4/mcm$. Its crystal structure is shown in figure 1. Notice that each layer of germanium atoms is a mirror image in [110] of its nearest-neighbour layers (a glide transformation). All germanium atoms lie in planes normal to [001] between the planes of iron atoms. The length of the *a*-axis is 5.908 Å and the length of the *c*-axis is 4.955 Å at room temperature. Hence, the distance between iron atoms is 2.478 Å along the *c*-axis and 4.178 Å in the (001) plane. The distance in the [001] direction is very close to the distance in elemental iron (2.86 Å). It is likely that the primary magnetic interaction along the *c*-axis is due to overlap of d orbitals, as it is in elemental iron, whereas the magnetic interaction in the plane is mediated by superexchange and the conduction electrons, leading to a net antiferromagnetic interaction. The low-temperature structure has ferromagnetic alignment of iron atoms along the *c*-axis chains and antiferromagnetic alignment between the chains, resulting in a collinear antiferromagnetic structure which is formed from two magnetic sublattices. The incommensurate SDW phase is characterized by four Bragg peaks displaced

from the commensurate (100) position along the (100) and (010) directions, similar to spin ordering observed in $La_2NiO_{4+\delta}$ [21] and $La_{2-x}Sr_xNiO_4$ [22], although in the latter case the correlations are short ranged. In the doped La_2NiO_4 the SDW ordering is coupled to charge-density-wave (CDW) ordering reflecting the strong coupling between charge and spin degrees of freedom in the transition metal oxides.

2. Experimental results and discussion

Single crystals of $FeGe_2$ were cut by spark erosion from the same sample as was employed in neutron scattering studies [23]. The samples were less than 1 mm in thickness and width and between 5 mm and 7 mm long. The resistance measurements were made using an AC resistance bridge with a frequency of 16 Hz. A platinum resistance thermometer was used for all of the high-temperature measurements and a carbon-glass thermometer was used for the low-temperature, high-magnetic-field measurements. The resistivity ratio ($\equiv \rho(300\ \mathrm{K})/\rho(0.3\ \mathrm{K})$) was 50 for all directions.

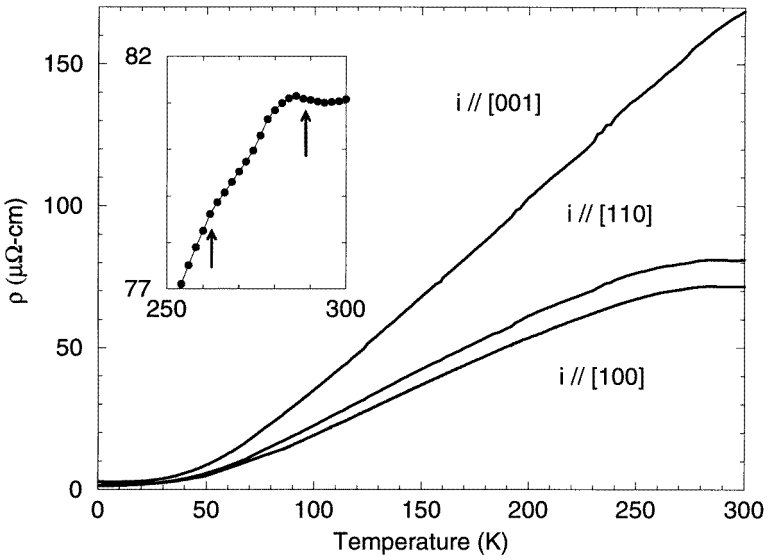

Figure 2. Resistivity as a function of temperature in zero field from 0.3 K to 300 K. Measurements for current ∥ [100], [110], and [001] are shown. Notice the large anisotropy between the in-plane and out-of-plane directions: the room temperature resistivities differ by a factor of 2. The inset highlights the phase transitions observed in measurements along [110].

The zero-field resistivity along [100], [110], and [001], measured between 0.3 K and 300 K, is shown in figure 2. Notice that there is a factor of two anisotropy between the basal-plane measurements and those along the *c*-axis and only moderate anisotropy in the basal plane itself. This is indicative of the difference between the atomic structure along the *c*-axis iron chains and the in-plane directions. The resistivity along the *c*-axis is remarkably linear between about 70 K and room temperature. The two phase transitions are well resolved as anomalies in the [110] data as shown by arrows in the inset to figure 2. The transition temperatures are $T_c = 263 \pm 2$ K and $T_N = 289 \pm 2$ K, in good agreement with those measured by neutron diffraction [9]. The [100] data show the transitions in a similar way. The data for current along [001], where the transitions are subtle, were not used in

the construction of the phase diagram. This difference between the signatures of the two transitions for in- and out-of-plane directions is not surprising since the propagation vector of the SDW and the direction of the magnetic moments lie in the basal plane, not along the c-axis. Error associated with the transition temperature values arises from uncertainty in locating the phase transition since the anomaly occurs over a rather large range and we do not have a theoretical prediction for $\rho(T)$ near the phase transitions where the phonon background is large. We define T_c as the knee of the $\rho(T)$ curve (the lower transition) and T_N as the inflection point of the $\rho(T)$ curve (the upper transition) yielding the same transition temperatures as reported by Corliss *et al* [9]. Our data are in fair agreement with those of Krentsis *et al* [12]. The compared values of room temperature resistivity are 167 ± 17 $\mu\Omega$ cm and 140 ± 5 $\mu\Omega$ cm for the c-axis and 72 ± 8 $\mu\Omega$ cm and 80 ± 3 $\mu\Omega$ cm along [100] for our results and those of Krentsis *et al* [12] respectively.

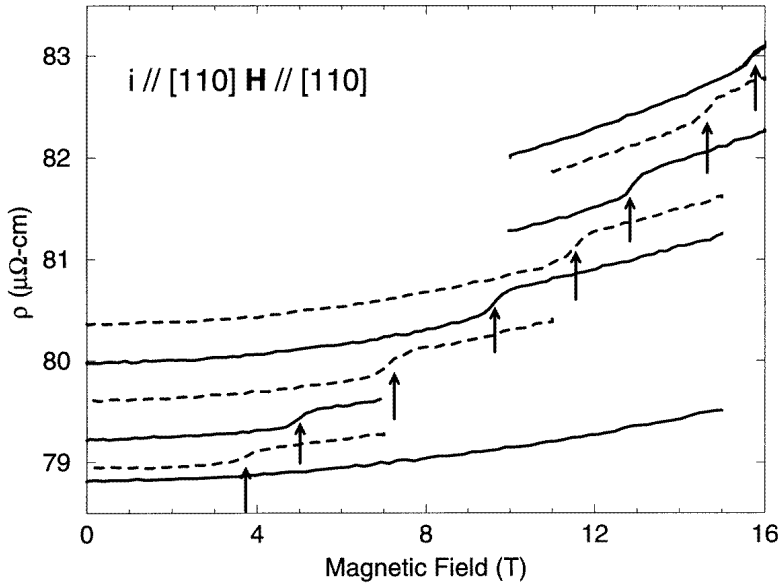

Figure 3. A set of magnetic field sweeps along [110] near the lower transition temperature T_c, showing the phase boundary. The temperatures are, from the bottom to the top, 260 K, 263.6 K, 264 K, 265 K, 266.1 K, 267 K, 267.7 K, 268.5 K, and 269 K. Transitions are shown by arrows. Notice the difference in the curve at 260 K where no transition is present. The uncertainty in $\mu_0 H$ at the transition is 0.2 T. The curves have been offset for the sake of clarity. The $T = 260$ K and the $T = 264$ K curve have not been shifted. The other curves have been shifted up or down by 0.25 $\mu\Omega$ cm for each step away from 264 K.

To investigate the magnetic phase diagram we performed field sweeps at constant temperature near the lower transition and temperature sweeps at constant field through both transitions. The temperature and magnetic field at the phase boundaries were measured at the point of the resistance anomaly in the sweep. The set of field sweeps along [110] near the lower transition is shown in figure 3. Both increasing and decreasing sweeps of magnetic field were performed. The phase transitions are marked by the inflection points of the resistance curves. The slight increase in resistivity upon going into the commensurate phase may be due to the formation of a new magnetic superzone, causing extra scattering of the charge carriers. The resulting magnetic phase diagram is shown in figure 4 along with

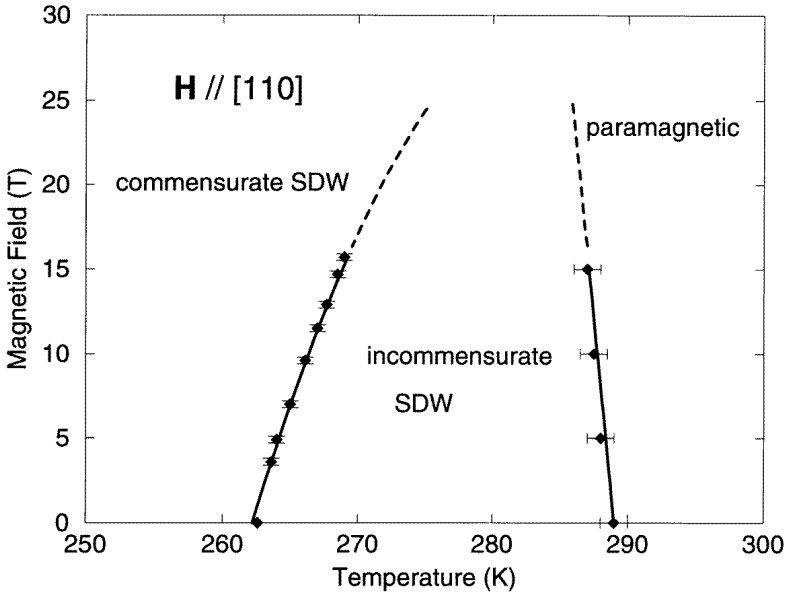

Figure 4. The magnetic phase diagram of $FeGe_2$ for $\boldsymbol{H} \parallel [110]$ constructed from data in figure 3 and temperature sweeps that are not shown. Solid lines are used in our experimental range up to 16 T. The dashed lines are a simple extrapolation to higher fields: $H(T)/H_c = 1-[(T-T_N(H_c))/(T_c-T_N(H_c))]^2$ for the C–IC transition and $H(T)/H_c = 1-T/(T_N(H_c)-T_N)$ for the Néel transition where $T_N(H_c)$ is the Néel temperature at the critical field. The phase diagrams for fields along [110] and [100] are virtually identical.

a simple (quadratic) extrapolation to higher magnetic fields. We found an identical phase diagram for fields in the [100] direction once again indicating the small anisotropy in the basal plane. The phases shown are the only ones present in the range of temperature (0.3–300 K) and magnetic field (0–16 T) accessed by our measurements. Future experiments, most likely specific heat measurements, are planned to verify this phase diagram. In figure 4 the Néel transition line shows a nearly vertical increase with field. However, T_c noticeably increases with magnetic field along [100] or [110] and has increased by 6 K in a magnetic field of 15 T. When we assume a quadratic dependence of $\boldsymbol{H}$ at the transition on T_c and a slight linear change in T_N we expect the IC phase to be stable up to a critical field of $\mu_0 H_c \simeq 30$ T.

In spite of the simplicity of the extrapolation involved it is obvious that the critical field is much larger than the 1 T predicted by Tarasenko *et al* [16]. The reason for this discrepancy is unclear at this time. These authors used a free-energy expansion in powers of the sublattice magnetization combined with a Landau–Khalatnikov analysis of the phase stability. This approach predicts that the incommensurate SDW phase contains longitudinal and transverse phases which are separated by a first-order transition. The longitudinal phase would be virtually invisible to experiment since it only exists over a narrow temperature range of 20 mK just below the Néel transition. This extra phase is required however if the Néel transition is second order [9] and the C–IC transition is first order [14]. One key approximation in the analysis of Tarasenko *et al* [16] is that the anisotropy between the in-plane directions is assumed to be zero and the anisotropy between the basal plane and c-axis is assumed to be infinite. Inelastic neutron scattering measurements of the spin waves

in the commensurate phase have found that the anisotropy in the magnetic interactions along [001] and [100] is about a factor of two [23]. Also, estimates had to be made for the coupling constants between the magnetic field and the fluctuations which appear in the Landau–Khalatnikov equations of motion. It is hoped that the new data as well as some of the concepts introduced by Corliss *et al* [9] with regard to the phase diagram will contribute towards a refined prediction that agrees with experiment. Such a refinement will be useful in determining the magnetic properties of related compounds with SDW transitions to commensurate or incommensurate phases such as gallium- or arsenic-doped $FeGe_2$ and $Cr + 0.2$ at.% V [24] and could also give insight into the interactions at work in the high-T_c oxides.

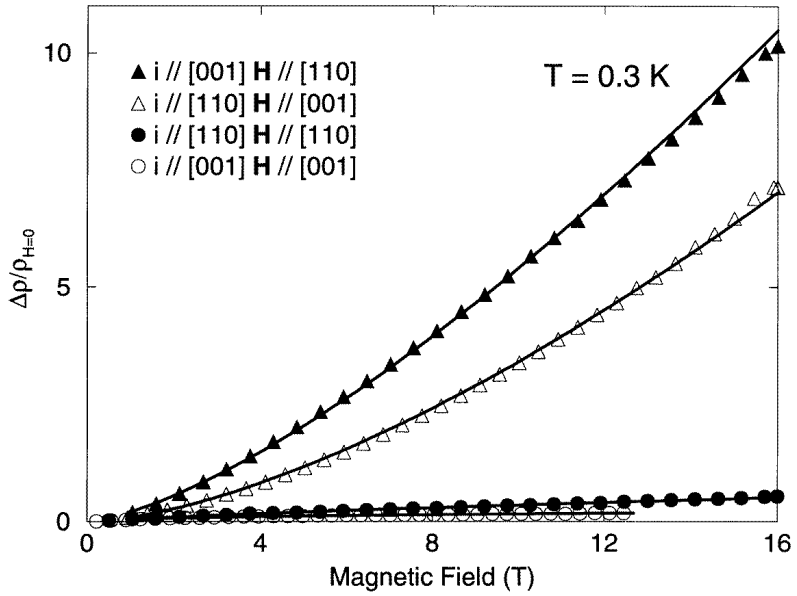

Figure 5. Magnetoresistance $\Delta\rho/\rho_{H=0}$ data for current along [110] and [001] for longitudinal and transverse magnetic fields. The solid lines are power laws $\Delta\rho/\rho_{H=0} \propto H^{\alpha}$ for fields greater than 1 T. The values of α are, from top to bottom, 1.41(5), 1.54(5), 0.79(6), and 0.48(6). The uncertainties arise from the variation in fit over different magnetic field ranges. Some data points have been omitted for clarity.

We have also performed low-temperature (0.3 K) magnetoresistance measurements in magnetic fields up to 16 T along the [001] and [110] directions in transverse and longitudinal configurations and also for current along [100] and magnetic field along [001]. All sets of transverse measurements show substantial magnetoresistance in high fields. The behaviour that we see is intermediate to closed orbits and open orbits since there is no saturation of magnetoresistance as one would expect for a closed orbit and no sample shows an H^2-dependence that would clearly signify an open orbit. The best description of the data between 1 T and 16 T is given by H^{α} with $\alpha < 2$ in all cases with the basal-plane transverse magnetoresistance giving values of α slightly less than 2. These fits for current along [110] and [001] along with the exponents, α, are shown in figure 5. Other descriptions of the field dependence, such as polynomials, were less successful for the same range of magnetic fields and the data shown. The observed transverse magnetoresistance could arise from a combination of closed and open orbits complicated by impurities in the sample. Band-

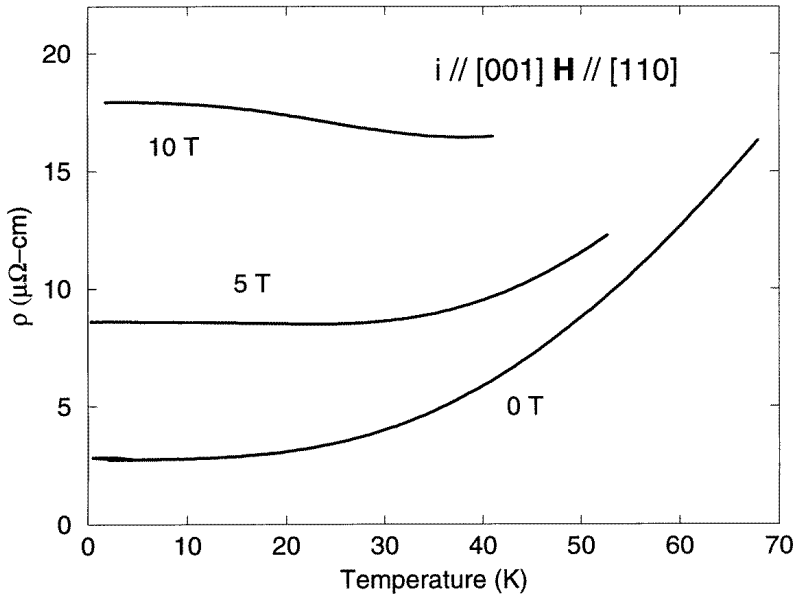

Figure 6. The variation in magnetoresistance with temperature for $\boldsymbol{i} \parallel [001]$ and $\boldsymbol{H} \parallel [110]$.

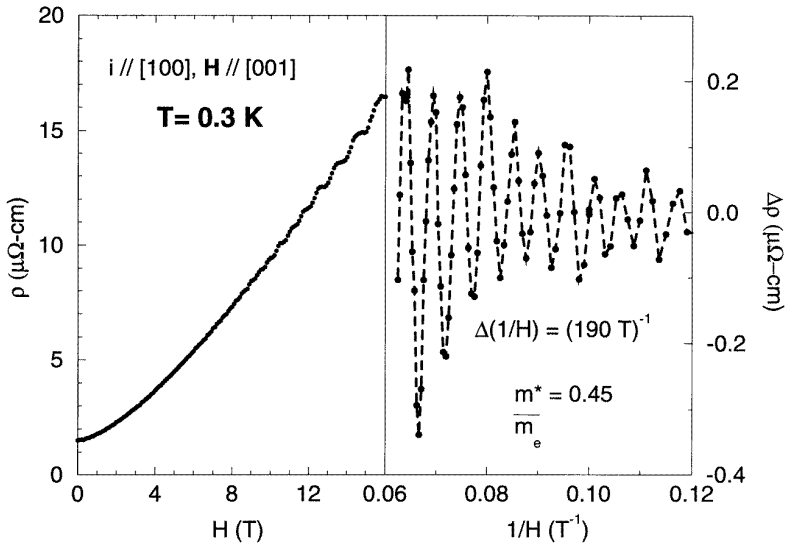

Figure 7. Resistivity for $\boldsymbol{i} \parallel [100]$ and $\boldsymbol{H} \parallel [001]$ versus magnetic field at 0.3 K. The panel on the left shows the raw data and the panel on the right highlights the quantum oscillations. The data pictured constitute the residual from a quadratic fit plotted versus $1/H$ giving a frequency of 190 ± 10 T and an effective mass of $0.45 \pm 0.05\ m_e$.

structure calculations [25] show a Fermi surface with two sheets and the absence of open orbits in the [110] and [001] directions with an open orbit along [100] near the (001) face of the zone boundary. The gross behaviour for $\boldsymbol{i} \parallel [100]$ is well described by a quadratic

function over the entire field range or a power law with $\alpha = 1.37$ for the range from 1 to 16 T. Another interesting feature of the [001] transverse magnetoresistance measurements is shown in figure 6 where the magnetoresistance at 10 T is higher than the resistance in zero field at 70 K and we can clearly see the decrease in the magnitude of the magnetoresistance with increasing temperature. This result is also suggestive of open orbits due to the effect of increasing temperature on Fermi surface sharpness.

The most striking feature of the low-temperature transverse magnetoresistance is the occurrence of Shubnikov–de Haas oscillations for $\boldsymbol{H} \parallel [001]$ and $\boldsymbol{i} \parallel [100]$. We show these oscillations in figure 7. They remain clearly visible up to 4 K and for magnetic fields as low as 7 T. They can also be detected in the $\boldsymbol{i} \parallel [110]$ and $\boldsymbol{H} \parallel [001]$ data but are not nearly so prominent. The frequency of oscillations is 190 ± 10 T corresponding to a Fermi surface extremal area of $(1.8 \pm 0.1) \times 10^{-2}$ Å^{-2}. Previous observations [20] had found frequencies for $\boldsymbol{H} \parallel [001]$ of 35 T and 1630 T. We found no evidence for these frequencies but, with our field resolution, the high value of magnetic field where the oscillations appeared, and the presence of the oscillations at 190 T it would have been very difficult to observe either of these frequencies. It is interesting to note that a circular cross section would give a diameter of 0.142 ± 0.004 a^* which is of the same order of magnitude as the degree of discommensuration (0.05 a^*) possibly identifying the part of the Fermi surface responsible for wavevector nesting in the incommensurate phase. By carefully examining the oscillations at various temperatures, T, and magnetic fields, H, using a model [26] for the amplitudes, A:

$$A \propto T\sqrt{H}\ \frac{\exp(-2\pi^2 m^* c k_B T'/e\bar{h}H)}{\sinh(2\pi^2 m^* c k_B T/e\bar{h}H)} \tag{1}$$

giving a Dingle temperature, T', of 1.2 ± 0.1 K and an effective mass, m^*, of 0.45 ± 0.05 electron masses. This effective mass is comparable with previous measurements [25] which gave a value of 0.51 ± 0.02 m_e for the high-frequency oscillation for $\boldsymbol{H} \parallel [001]$. The appearance of strong oscillations in the transverse magnetoresistance is another indicator that the large magnetoresistance is due to a Fermi surface effect rather than the response of the magnetic structure to the applied field. Given the large Néel temperature and the large value of the critical field [16] it is unlikely that the magnetic fields used could cause such a substantial change in the resistivity (15 $\mu\Omega$ cm at 16 T) when at the phase transitions themselves we only see a change of less than one per cent (0.25 $\mu\Omega$ cm).

In conclusion, we have determined the magnetic phase diagram of the itinerant SDW antiferromagnet $FeGe_2$ for fields up to 16 T in the basal plane. The incommensurate phase that separates the paramagnetic from the commensurate phase is stable up to $\sim$30 T, in disagreement with predictions based on a Landau theory. Experimental determination of exchange and anisotropy constants and perhaps refinement of the approximations in the theory are necessary to resolve this inconsistency. Magnetization and neutron scattering experiments along these lines are planned for the near future. The low-temperature magnetoresistance shows a moderate anisotropy between the c-axis and the basal plane. The transverse magnetoresistance can be qualitatively understood on the basis of the reported band-structure. The appearance of a new frequency of quantum oscillations at 190 ± 10 T has identified a section of the Fermi surface that is of the same order of magnitude ($(1.8 \pm 0.1) \times 10^{-2}$ Å^{-2}) as that for Fermi surface nesting of the incommensurate spin-density wave. This provides an important clue to the connection between the magnetic structure and electronic structure. The effective carrier mass is in agreement with previous measurements of other extremal orbits in this material.

Acknowledgments

We are grateful to Professor A Z Menshikov for providing the single-crystal samples which were prepared at the Ural Polytechnical University, and J M Perz and T M Holden for helpful discussions. This work was supported by the Natural Sciences and Engineering Research Council of Canada and the Canadian Institute for Advanced Research.

References

[1] Takagi H, Ido T, Ishibashi S, Uota M, Uchida S and Tokura Y 1989 *Phys. Rev.* B **40** 2254
[2] Scalapino D J, Loh E Jr and Hirsch J E 1987 *Phys. Rev.* B **35** 6694
[3] Monthoux P, Balatsky A V and Pines D 1992 *Phys. Rev.* B **46** 14 803
[4] Levin K, Zha Y, Radtke R J, Si Q, Norman M R and Schüttler H-B 1994 *J. Supercond.* **7** 563
[5] Ruvalds J, Rieck C T, Tewari S, Thoma J and Virosztek A 1995 *Phys. Rev.* B **51** 3797
[6] Fawcett E, Alberts H L, Galkin V Yu, Noakes D R and Yakhmi J V 1994 *Rev. Mod. Phys.* **66** 25
[7] Bao W, Broholm C, Carter S A, Rosenbaum T F and Aeppli G 1993 *Phys. Rev. Lett.* **71** 766
[8] Walbaum H J 1943 *Z. Metallk.* **35** 218
[9] Corliss L M, Hastings J M, Kunnmann W, Thomas R, Zhuang J, Butera R and Mukamel D 1985 *Phys. Rev.* B **31** 4337
[10] Dorofeyev Yu A, Menshikov A Z, Budrina G L and Syromyatnikov V N 1987 *Phys. Metall. Metalloved.* **63** 62
[11] Menshikov A Z, Dorofeyev Yu A, Budrina G L and Syromyatnikov V N 1988 *J. Magn. Magn. Mater.* **73** 211
[12] Krentsis R P, Mikhel'son A V and Gel'd P V 1970 *Sov. Phys.–Solid State* **12** 727
[13] Krentsis R P, Meizer K I and Gel'd P V 1973 *Sov. Phys.–Solid State* **14** 2601
[14] Pluznikov V, Feder D and Fawcett E 1982 *J. Magn. Magn. Mater.* **27** 343
[15] Mikhel'son A V, Krentsis R P and Gel'd P V 1971 *Sov. Phys.–Solid State* **12** 1979
[16] Tarasenko V V, Pluzhnikov V and Fawcett E 1989 *Phys. Rev.* B **40** 471
[17] Menshikov A Z 1988 *Physica* B **149** 249
[18] Zainullina R I, Vlasov K B, Milyaev M A, Ustelemova E V and Syromyatnikov V N 1989 *Phys. Status Solidi* b **155** 419
[19] Piratinskaya I I, Mikhel'son A V and Krentsis R P 1979 *Sov. Phys.–Solid State* **21** 1050
[20] Svechkarev I V, Fawcett E and Holroyd F W 1980 *Solid State Commun.* **35** 297
[21] Tranquada J M, Buttrey D J, Sachan V and Lorenzo J E 1994 *Phys. Rev. Lett.* **73** 1003
[22] Hayden S M, Lander G H, Zaretsky J, Brown P J, Stassis C, Metcalf P and Honig J M 1992 *Phys. Rev. Lett.* **68** 1061
[23] Holden T M, Menshikov A Z and Fawcett E 1996 *J. Phys.: Condens. Matter* **8** L291
[24] Noakes D R, Holden T M, Fawcett E and de Camargo P C 1990 *Phys. Rev. Lett.* **65** 369
[25] Grechnev G E, Kübler J and Svechkarev I V 1991 *J. Phys.: Condens. Matter* **3** 7199
[26] Shonenberg D 1984 *Magnetic Oscillations in Metals* (New York: Cambridge University Press) pp 153–5